Crystal structure of botulinum neurotoxin type A and implications for toxicity

D. Borden Lacy[1], William Tepp[2], Alona C. Cohen[1], Bibhuti R. DasGupta[2] and Raymond C. Stevens[1]

Botulinum neurotoxin type A (BoNT/A) is the potent disease agent in botulism, a potential biological weapon and an effective therapeutic drug for involuntary muscle disorders. The crystal structure of the entire 1,285 amino acid di-chain neurotoxin was determined at 3.3 Å resolution. The structure reveals that the translocation domain contains a central pair of α-helices 105 Å long and a ~50 residue loop or belt that wraps around the catalytic domain. This belt partially occludes a large channel leading to a buried, negative active site — a feature that calls for radically different inhibitor design strategies from those currently used. The fold of the translocation domain suggests a mechanism of pore formation different from other toxins. Lastly, the toxin appears as a hybrid of varied structural motifs and suggests a modular assembly of functional subunits to yield pathogenesis.

The clostridial neurotoxin family is composed of tetanus neurotoxin and seven serotypes of botulinum neurotoxin (BoNT/A–BoNT/G). Botulinum neurotoxin serotype A is synthesized in *Clostridium botulinum* as a ~150,000 M_r single chain protein (1,296 amino acids). The toxin is post-translationally proteolyzed to form a 1,285 amino acid di-chain molecule in which the two chains, ~50,000 M_r and ~100,000 M_r, remain linked by a disulfide bond[1]. The protein is composed of three ~50,000 M_r functional domains where the catalytic function is confined to the ~50,000 M_r chain (residues 1–437), the translocation activity with the N-terminal half of the ~100,000 M_r chain (residues 448–872), and receptor binding with its C-terminal half (residues 873–1,295)[1,2]. The toxicity of BoNT is a result of a multi-step mechanism[3]. The neurotoxin binds to the pre-synaptic nerve endings of cholinergic neurons and enters by receptor-mediated endocytosis. Acidity in the endosome is believed to induce pore formation, which allows translocation of the catalytic domain into the cytosol. The zinc-dependent catalytic domain of the seven BoNT serotypes specifically cleaves one of three different SNARE proteins essential for synaptic vesicle fusion: synaptobrevin, syntaxin, or SNAP-25. This cleavage results in inhibition of acetylcholine secretion, ultimately leading to paralysis[1].

What remains unknown is how the highly homologous BoNT serotypes and tetanus toxin derive specificity both for different receptors and their different SNARE protein targets. Furthermore, a number of questions surround the mechanism by which a soluble protein changes with acidic pH to one that can span a membrane and translocate a ~50,000 M_r protein into the cytoplasm . We describe here the crystal structure of BoNT/A and then use this structural information to address some of these mechanistic questions.

Overall structure of BoNT/A

The crystal structure of BoNT/A was determined by multiple isomorphous replacement (MIR) using five heavy-atom derivatives (Table 1). Phases were further improved with solvent flattening to yield readily interpretable electron density maps (Fig. 1). The model, which includes 99% of the amino acids, was refined to 3.3 Å with an R-value of 20.0% and an R_{free} value of 27.9%. The BoNT/A molecule is approximately 45 Å × 105 Å × 130 Å and shows a linear arrangement of the three functional domains with no contact between the catalytic and binding domains (Fig. 2). In general, the three functional domains are also structurally distinct. The exception is an unusual loop, or belt, from what has historically been considered part of the translocation domain, that wraps around the perimeter of the catalytic domain.

Fig. 1 Stereo diagram of the initial electron density. The map was calculated with MIR phases extended to 3.6 Å, improved by density modification, and contoured at 2.0σ. This region of the structure corresponds to the pair of α-helices in the translocation domain.

[1]Department of Chemistry and Earnest Orlando Lawrence Berkeley National Laboratory, University of California, Berkeley, California 94720, USA. [2]Department of Food Microbiology and Toxicology, University of Wisconsin, Madison, Wisconsin 53706, USA.

Correspondence should be addressed to R.C.S. *e-mail: stevens@adrenaline.berkeley.edu*

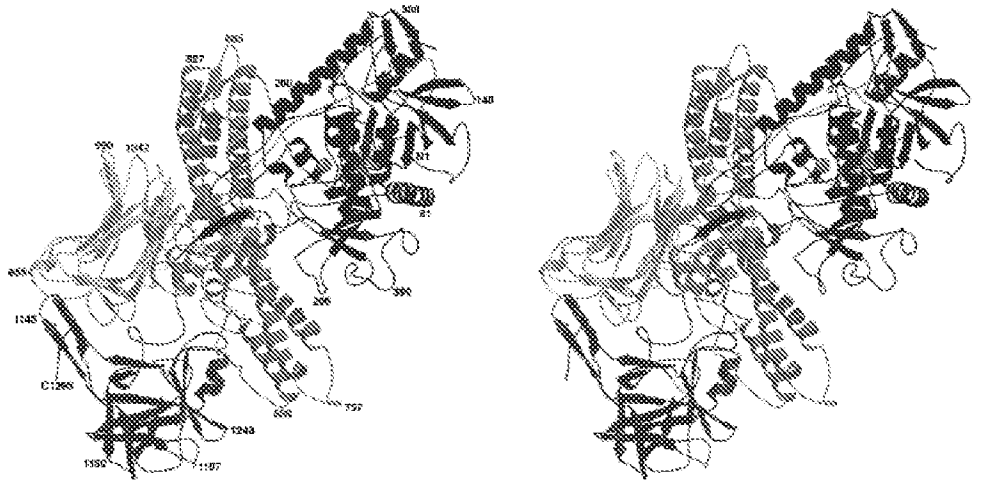

Fig. 2 Stereo diagram of the backbone trace for the BoNT/A model. The catalytic domain is colored in blue, the translocation domain in green, the N-terminal binding sub-domain in yellow and the C-terminal binding sub-domain in red. The catalytic zinc is depicted as a ball in gray. The 'X' dictates the proteolytic site separating the two chains. The dashed line is the only loop region with ill-defined electron density. The lower view shows the model rotated ~90° out of the plane of the page relative to the top view and should better depict the translocation domain belt wrapping around the catalytic domain. The overall structure is 45 Å × 105 Å × 130 Å. Figure generated using MOLSCRIPT[36].

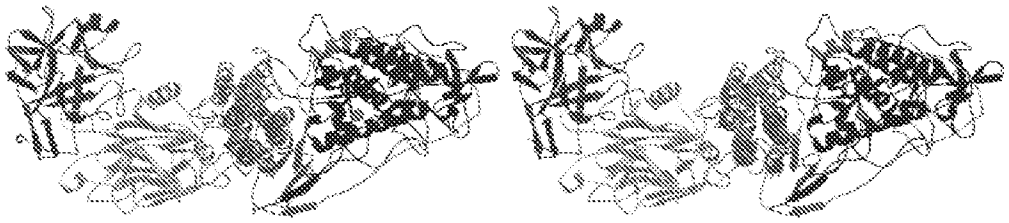

Receptor binding domain

The binding domain, with overall dimensions of 32 Å × 37 Å × 76 Å, appears as two distinct sub-domains roughly equal in size. Both sub-domains are composed predominantly of β-strands and are connected by one prominent α-helix. The N-terminal sub-domain has two seven-stranded β-sheets sandwiched together in a jelly roll motif with dimensions 32 Å × 37 Å × 38 Å. The C-terminal sub-domain has similar dimensions and adopts a modified β-trefoil fold with a six-stranded β-barrel next to the N-terminal jelly roll motif and a β-hairpin triplet capping the base of the domain. The entire binding domain tilts away from the long helical axis of the translocation domain such that there is no contact between the C-terminal sub-domain and the translocation domain and all of the surface loops are accessible for binding. The binding domain shares structural homology with the recently solved structure of the tetanus toxin binding domain[4] with an r.m.s. deviation of 1.5 Å for 363 Cα positions (Fig. 3). The major differences appear in the loops of the C-terminal sub-domain, where the longer loop lengths in the tetanus toxin sub-domain account for the domain's slightly longer length in primary sequence.

The first step in the intoxication mechanism is a binding event between the binding domain and the pre-synaptic nerve ending. The interaction with BoNT/A is proposed to occur through both a polysialoganglioside (G_{D1b} or G_{T1b}) and a yet unidentified protein receptor[5,6]. The putative ganglioside binding site for tetanus neurotoxin, as assessed by photoaffinity labelling[7], is in a loop of the C-terminal sub-domain, and when overlayed with the BoNT/A holotoxin structure, is fully accessible. This could represent a general ganglioside binding site for all the clostridial neurotoxins. It is striking that both sub-domains have structural homology with proteins known to interact with sugars — as assessed using Dali[8], a three-dimensional search algorithm — and its ranked output according to Z-score. (The Z-score is the strength of structural similarity in

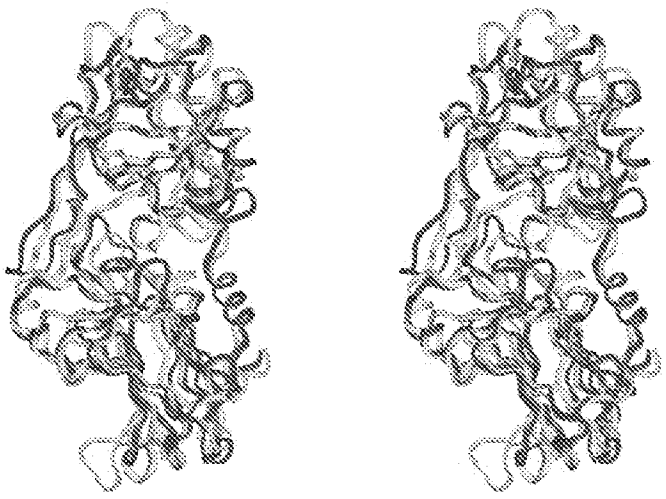

Fig. 3 Stereo superposition of the BoNT/A binding domain (residues 873–1,295) in red and the tetanus toxin binding domain (residues 874–1,314) in yellow. The root-mean-square (r.m.s.) deviation is 1.5 Å for 363 Cα atoms. The major structural differences are in the C-terminal sub-domain loops.

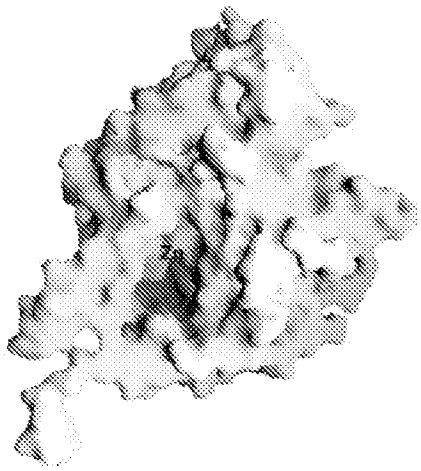

Fig. 4 Molecular surface of the catalytic domain colored by electrostatic potential (red = negative, blue = positive, white = uncharged). The active site is buried within the channel and appears largely negative. In the holotoxin, this pocket is partially blocked by the translocation domain belt. Figure generated using GRASP[37].

standard deviations over the expected where pairs with Z < 2 are structurally dissimilar.) The top twelve proteins after tetanus toxin (Z = 26.3) that are structurally similar to the N-terminal sub-domain are proteins known to interact with sugars (for example, serum amyloid P (1sac-A, Z = 12.8), β-glucanase (2ayh, Z = 11.1), sialidase (1kit, Z = 8.9), and lectin (1led, Z = 8.8)). Perhaps the most notable of these twelve are cryia (1ciy, Z = 5.2) and insecticidal ∂-endotoxin (1dlc, Z = 4.8) which act by binding glycoproteins and creating leakage channels[9]. These toxins have binding domains with motifs similar to the N-terminal sub-domain of BoNT/A but dramatically different pore-forming domains. A Dali search of the C-terminal sub-domain reveals more sugar binding proteins (basic fibroblast growth factor (1bfg, Z = 9.1), agglutinin (1jly-A, Z = 9.9)) and the toxin abrin (1abr-B, Z = 8.8). Both abrin and the related ricin bind their targets through a β-trefoil binding domain. The appearance of different subsets of the same structural motifs in different toxins could suggest a mechanism of evolution in which stable functional domains are assembled as modular units giving rise to toxicity.

Pore-formation and translocation domain

Following cell surface binding and receptor-mediated endocytosis of the neurotoxin, an acid-induced conformational change in the neurotoxin's translocation domain is believed to allow the translocation domain to penetrate the endosome and form a pore. The membrane interaction and pore formation is thought to facilitate the passage of the catalytic domain across the membrane into the cytosol. The details of how the translocation domain changes conformation at acidic pH to form a pore and how it can allow for the passage of a 50,000 M_r catalytic domain across the endosomal membrane are the least understood aspects of the intoxication mechanism. To date, most investigations of the translocation event in BoNT have assumed a similarity to other pH dependent α-helical pore-forming proteins: diphtheria toxin, colicin A, δ-endotoxin, pseudomonas exotoxin, and Bcl-x_L[9-13]. These proteins share a common structural motif in their pore forming domain[13,14], however this motif is not observed in the BoNT/A structure.

The translocation domain of BoNT/A wraps around the catalytic domain before forming its main body, a cylindrical shape with dimensions of 28 Å × 32 Å × 105 Å (Fig. 2). The most salient feature of the translocation domain is a pair of α-helices 105 Å long corresponding to residues 685–827. While unusual, long pairs of α-helices have been observed recently in the structures of colicin Ia[15] and the nucleotide exchange factor GrpE[16]. The helices, anti-parallel and amphipathic, twist around each other like a coiled coil but do not adhere to a strict heptad repeat. At both ends of this pair of helices, a shorter α-helix packs in parallel to the long helical axis. In addition, the domain has two strand-like sections which pack against the pair of α-helices in a parallel fashion. In an effort to identify the pore-forming segment of BoNT/A, the primary sequence was searched for predicted amphipathic helicity, and the candidate segment (residues 659–681) was shown to increase permeability of lipid bilayers[17]. The present structure, solved at neutral pH, shows that none of this putative transmembrane segment is helical and that, in fact, part of it appears to be in one of the two strand-like segments packing against the long α-helices. This could indicate an area that will undergo structural changes with pH. However, the

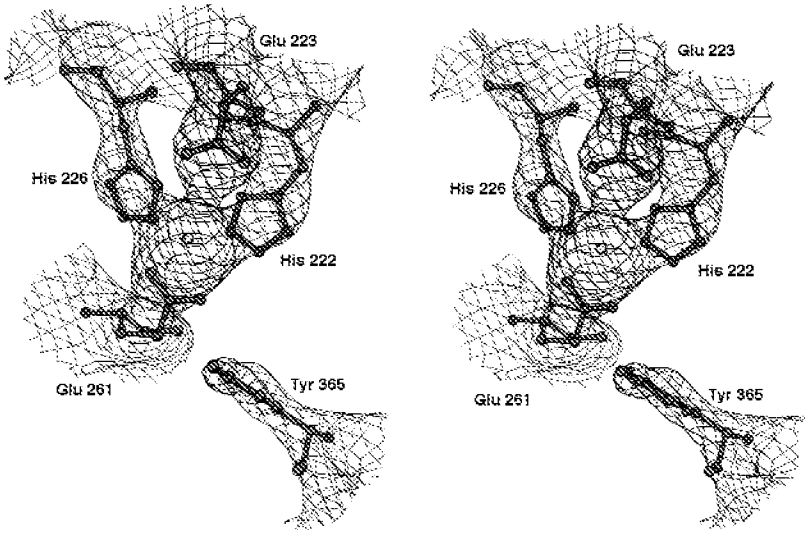

Fig. 5 Stereo diagram of the catalytic domain active site. A σ_A-weighted F_{obs} - F_{calc} omit map contoured at 2.6σ and centered around the zinc shows the amino acids (green carbon, red oxygen, and blue nitrogen bonds) thought to be critical for full catalytic activity. Figure generated using BOBSCRIPT.

Table 1 Structure determination statistics

Diffraction data statistics

Crystal	Resolution (Å)	Total obs.	Unique refl.	Completeness[1] (%)	R_{merge}[2] (%)
Native	20–3.3	172,169	40,110	98.2(94.3)	11.1(48.3)
CH_3HgCl	15–4.5	87,457	15,830	97.2(96.0)	10.7(27.7)
$Hg_2(Ac)_2$	15–4.2	86,260	19,650	97.8(94.3)	9.1(24.5)
SmAc	15–4.5	22,797	12,516	78.5(78.2)	7.6(17.4)
UAc	15–4.5	22,795	11,796	71.9(73.6)	7.8(22.5)
$KAuCl_4$	15–6.0	19,894	6,080	93.7(95.5)	9.4(18.2)

Phasing statistics

Derivative	Number of sites[3]	Isomorphous R-factor[4] (%)	Phasing power[5] Cent.	Phasing power[5] Acent.	R_{Cullis}[6] Cent.	R_{Cullis}[6] Acent.
CH_3HgCl	6	21.7	1.03	1.64	0.68	0.65
$Hg_2(Ac)_2$	6	21.0	0.96	1.36	0.76	0.76
SmAc	3	14.9	0.77	1.07	0.83	0.87
UAc	3	15.2	0.66	1.04	0.88	0.91
$KAuCl_4$	1	15.2	0.63	1.03	0.88	0.88
FOM before solvent flattening (15–3.6 Å)		0.48				
FOM after solvent flattening (15–3.6 Å)		0.74				

Refinement statistics

R-factor/R_{free}	20.0/27.9
R.m.s.d. bond lengths	0.008 Å
R.m.s.d. bond angles	1.5°

[1]Numbers in parentheses indicate statistics for highest resolution shells.
[2]$R_{merge} = \Sigma_h\Sigma_i | I_{hi} - \langle I_{hi}\rangle | / \Sigma_h\Sigma_i | I_{hi} |$, where h specifies unique indices, i indicates symmetry equivalent observations of h, and $\langle I_{hi}\rangle$ is the mean value.
[3] The mercury and gold derivatives shared overlapping sites. Similarly, the samarium and uranyl derivatives shared sites. However, the different occupancies yielded enough new phase information to improve the quality of the maps.
[4]The isomorphous R-factor = $\Sigma_h || F_{ph} | - | F_p | / \Sigma_h | F_p |$, where $| F_{ph} |$ and $| F_p |$ are the measured structure factor amplitudes of the derivative and native structures.
[5]Phasing power is the mean value of the heavy atom structure factor amplitude divided by the residual lack of closure error.
[6]R_{Cullis} is the mean residual lack of closure error divided by the isomorphous difference.

residues most likely to titrate over this pH range are the two histidines in the translocation domain, which are located some distance from this region of the structure: His 551 and His 560 are found in a loop between the translocation domain belt and the main body of the translocation domain. This junction may play a role in exposing a hydrophobic segment of the protein or releasing the catalytic domain from the translocation domain. Regardless of the pore-forming segment location, it is clear that the translocation domain of BoNT/A is structurally distinct from the other pore-forming toxins. In fact, the long pair of α-helices with their triple helix bundles at either end bear more resemblance to the coiled coil viral proteins: HIV-1 gp41/GCN4, influenza hemagglutinin, and the MoMuLV TM fragment[18–20]. These proteins do not translocate through pores but do have an acid-induced ability to undergo structural changes and penetrate membranes.

Catalytic domain

Either within the acidic endosome or upon exposure to the cytosol following translocation, the disulfide bond connecting the catalytic and translocation domains (Cys 429–Cys 453) is reduced, and the catalytic domain is released into the cytoplasm. The catalytic domain, 55 Å × 55 Å × 62 Å, is a mixture of both α-helix and β-strand secondary structure, in agreement with secondary structure predictions[21]. The active site of the catalytic domain is buried 20–24 Å deep in the protein, has a negative surface charge, and is accessible by a channel, ~12 Å × 15 Å × 35 Å, (Fig. 4). In the di-chain holotoxin, this channel is partially shielded from solvent by both the belt and the main body of the translocation domain.

The final mechanistic step in toxicity is the cleavage of a presynaptic protein by the BoNT zinc protease catalytic domain. The catalytic zinc atom represents the highest peak in the electron density maps and is visible in MIR maps contoured at 7.5σ. Amino acids with side chains closest to the zinc include His 222, Glu 223, His 226, Glu 261 and Tyr 365 (Fig. 5). While the presence of His 222, Glu 223 and His 226 was anticipated[1], this structure identifies Glu 261 as the fourth ligand, and may help resolve uncertainty in tetanus toxin where either Glu 269 or Glu 270 had been implicated[22]. (Glu 269 and Glu 270 of tetanus toxin align to Glu 260 and Glu 261 of BoNT/A). Further, while the role of a tyrosine was anticipated[23,24], the structure indicates that it is the conserved Tyr 365 and not the conserved Tyr 232 which is within proximity to the zinc. While exact bond lengths and water molecules cannot be confirmed at this resolution, the observed orientation of these residues support a model in which the His 222, His 226 and Glu 261 directly coordinate the zinc, and Glu 223 coordinates a water molecule as the fourth ligand. The Tyr 365 residue is ~5 Å from the zinc (OH–Zn) and is more likely to be involved in secondary bonding networks or interaction with substrate. A Dali search[8] shows that the proteins with the most structural similarity to the catalytic domain are thermolysin (1hyt, Z = 4.6) and leishmanolysin (1lml, Z = 2.4), two other zinc proteases with the same conserved HEXXH sequence. The structural similarities are limited, however, to the helix containing the HEXXH sequence and a four-stranded β-sheet buttressing the helix. Beyond this overlap, the BoNT/A catalytic domain has different secondary structure elements and connectivities.

The catalytic domain of BoNT/A is highly specific for the C-terminus of SNAP-25 and appears to require a minimum of

16 substrate amino acids for cleavage[25]. This large substrate size requirement is unusual for metalloproteases. The molecular recognition properties between the toxin and SNAP-25 and the dependence of recognition on a specific substrate secondary structure is presently being investigated[26,27]. The channel (~12 Å × 15 Å × 35 Å) leading to the active site (Fig. 4) appears capable of accommodating 16 or more residues with the Gln–Arg cleavage site of SNAP-25 able to insert into the zinc catalytic site. Additionally, the high pI of SNAP-25's C-terminal tail suggests that the negatively charged surface observed near the active site could be critical in the docking of substrate. Interestingly, the active site is most accessible in the absence of the translocation domain. This structure, in which the translocation domain shields the active site in the unreduced holotoxin, explains the fact that the catalytic activity in *in vitro* experiments is greatly enhanced by reduction of the disulfide. This observation of an occluded active site, along with the characterization of the amino acid environment, will almost certainly benefit ongoing inhibitor design.

Methods

Crystals were grown as described[28], but with a modified mother liquor of 150 mM magnesium acetate, 11% PEG 4000, and 100 mM tris-HCl pH 7. The crystals contain one monomer per asymmetric unit and are in space group $P3_121$ (a = b = 170.5 Å, c = 161.1 Å) with a solvent content of 70%. Derivatives were prepared by soaking crystals in: 1 mM potassium tetrachloroaurate for 8–12 h, 1 mM mercurous acetate for 6 h, 3 mM methyl mercuric chloride for 6 h, 50 mM samarium acetate for 12 h, or 0.5 mM uranyl acetate for 6–10 h. Diffraction data for native and derivatized crystals were collected at 4 °C at SSRL, beamline 7-1 and beamline 9-1, at 1.08 Å and 0.98 Å respectively. Crystals diffracted reasonably well for about five images using 1° oscillations before showing signs of radiation damage. Taking advantage of the high symmetry and the ability to translate bar shaped crystals allowed for complete data sets to be collected from a few crystals. All data were processed with DENZO and SCALEPACK[29], allowing for decreased resolution and increased mosaicity as the crystal decayed. The CCP4 suite of programs[30] was used for scaling the data sets and locating the heavy atom positions. Patterson maps were viewed with XCONTUR[31]. MLPHARE[30] was used for heavy-atom position refinement and phase calculation. Phases were extended to 3.6 Å and improved by solvent flattening and histogram matching using the program DM[32]. The model was built to 3.6 Å resolution using the program O[33], and then, as more data was collected, extended to 3.3 Å. Maps were improved with phase combination using SIGMAA[34]. Cycles of rebuilding, positional refinement, and simulated annealing using X-PLOR[35] were continued until convergence. Excellent electron density exists throughout the model and 99% of the amino acids were visible. Not surprisingly, the two ill-defined regions of the structure are the site of proteolytic cleavage between the two chains and in a surface loop immediately following His560 of the translocation domain.

Coordinates. Coordinates have been deposited in the Brookhaven Protein Data Bank (accession number 3bta).

Acknowledgments

We thank M. Evenson, B. Santarsiero, B. Spiller and G. Wedemayer for their help in the project, P. Kuhn and M. Soltis for their assistance at beamlines 7-1 and 9-1 at the Stanford Synchrotron Radiation Laboratory, R. Sweet at beamline X12C of the Brookhaven National Laboratory, T. Earnest at the Advanced Light Source, F. Lebeda for helpful discussions, and T. Umland for providing us with the tetanus toxin binding domain coordinates. Financial support for this research was provided by a NSF pre-doctoral fellowship (D.B.L.) and the US Army Medical Research Institute of Infectious Diseases.

Received 25 June 1998; accepted 7 July 1998.

1. Montecucco, C. & Schiavo, G. Structure and function of tetanus and botulinum neurotoxins. *Quarterly Rev. Biophys.* **28**, 423–472 (1995).
2. Krieglstein, K. G., DasGupta, B. R. & Henschen, A. H. Covalent structure of botulinum neurotoxin type A: location of sulfhydryl groups, and disulfide bridges and identification of C-termini of light and heavy chains. *J. Prot. Chem.* **13**, 49–57 (1994).
3. Simpson, L. L. Kinetic studies on the interaction between botulinum toxin type A and the cholinergic neuromuscular junction. *J. Pharmacol. Exp. Ther.* **212**, 16–21 (1980).
4. Umland, T. C. *et al.* Structure of the receptor binding fragment Hc of tetanus neurotoxin. *Nature Struct. Biol.* **4**, 788–792 (1997).
5. Nishiki, T. *et al.* The high-affinity binding of *Clostridium botulinum* type B neurotoxin to synaptotagmin II associated with gangliosides GT1b/GD1a. *FEBS Lett.* **378**, 253–257 (1996).
6. Montecucco, C. How do tetanus and botulinum toxins bind to neuronal membranes? *TIBS* **11**, 314–317 (1986).
7. Shapiro, R. E. *et al.* Identification of a ganglioside recognition domain of tetanus toxin using a novel ganglioside photoaffinity ligand. *J. Biol. Chem.* **272**, 30380–30386 (1997).
8. Holm, L. & Sander, C. The FSSP database of structurally aligned protein fold families. *Nucleic Acids Res.* **22**, 3600–3609 (1994).
9. Li, J. D., Carroll, J. & Ellar, D. J. Crystal structure of insecticidal delta-endotoxin from *Bacillus thuringiensis* at 2.5 Å resolution. *Nature* **353**, 815–821 (1991).
10. Choe, S. *et al.* The crystal structure of diphtheria toxin. *Nature* **357**, 216–222 (1992).
11. Parker, M. W., Pattus, F., Tucker, A. D. & Tsernoglou, D. Structure of the membrane-pore-forming fragment of colicin A. *Nature* **337**, 93–96 (1989).
12. Allured, V. S., Collier, R. J., Carroll S. F. & McKay, D. B. Structure of exotoxin A of *Pseudomonas aeruginosa* at 3.0-Angstrom resolution. *Proc. Natl. Acad. Sci. U. S. A.* **83**, 1320–1324 (1986).
13. Muchmore, S. W. *et al.* X-ray and NMR structure of human Bcl-x_L, an inhibitor of programmed cell death. *Nature* **381**, 335–341 (1996).
14. Parker, M. W. & Pattus, F. Rendering a membrane protein soluble in water: a common packing motif in bacterial protein toxins. *Trends Biochem. Sci.* **18**, 391–395 (1993).
15. Wiener, M., Freymann, D., Ghosh, P. & Stroud, R. M. Crystal structure of colicin Ia. *Nature* **385**, 461–464 (1997).
16. Harrison, C. J., Hayer-Hartl, M., Di Liberto, M., Hartl, F. & Kuriyan, J. Crystal structure of the nucleotide exchange factor GrpE bound to the ATPase domain of the molecular chaperone DnaK. *Science* **276**, 431–435 (1997).
17. Oblatt-Montal, M., Yamazaki, M., Nelson, R. & Montal, M. Formation of ion channels in lipid bilayers by a peptide with the predicted transmembrane sequence of botulinum neurotoxin A. *Protein Science* **4**, 1490–1497 (1995).
18. Weissenhorn, W., Dessen, A., Harrison, S. C., Skehel, J. J. & Wiley, D. C. Atomic structure of the ectodomain from HIV-1 gp41. *Nature* **387**, 426–430 (1997).
19. Bullough, P. A., Hughson, F. M., Skehel, J. J. & Wiley, D. C. Structure of influenza haemagglutinin at the pH of membrane fusion. *Nature* **371**, 37–43 (1994).
20. Fass, D., Harrison, S. C. & Kim, P. S. Retrovirus envelope domain at 1.7 Å resolution. *Nature Struct. Biol.* **3**, 465–469 (1996).
21. Lebeda, F.J. & Olson, M.A. Secondary structural predictions for the clostridial neurotoxins. *Proteins: Struct. Funct. Genet.* **20**, 293–300 (1994).
22. Yamasaki, S. *et al.* Synaptobrevin/vesicle-associated membrane protein (VAMP) of *Aplysia californica*: structure and proteolysis by tetanus toxin and botulinal neurotoxins type D and F. *Proc. Natl. Acad. Sci. USA* **91**, 4688–4692 (1994).
23. Woody, M. & DasGupta, B. R. Effect of tetranitromethane on the biological activities of botulinum neurotoxin types A, B, and E. *Mol. Cell. Biochem.* **85**, 159–169 (1989).
24. Morante, S. *et al.* X-ray absorption spectroscopy study of zinc coordination in tetanus neurotoxin, astacin, alkaline protease and thermolysin. *Eur. J. Biochem.* **235**, 606–612 (1996).
25. Schmidt, J. J. & Bostian, K. A. Endoproteinase activity of type A botulinum neurotoxin: substrate requirements and activation by serum albumin. *J. Protein Chem.* **16**, 19–26 (1997).
26. Rossetto, O. *et al.* The metallo-proteinase activity of tetanus and botulinum neurotoxins. *J. Physiology (Paris)* **89**, 43–50 (1995).
27. Schmidt, J. J. & Bostian, K. A. Proteolysis of synthetic peptides by type A botulinum neurotoxin. *J. Protein Chem.* **14**, 703–708 (1995).
28. Stevens, R. C., Evenson, M. L., Tepp, W. & DasGupta, B. R. Crystallization and preliminary x-ray analysis of botulinum neurotoxin type A. *J. Mol. Biol.* **222**, 877–880 (1991).
29. Otwinowski, Z., in *Data Collection and Processing*, (eds Sawyer, L., Isaacs, N. & Bailey, S.) 56–62 (Science and Engineering Research Council, Warrington, UK; 1993).
30. *CCP4: A Suite of Programs for Protein Crystallography* (SERC Daresbury Laboratory, Warrington WA4 4AD, UK; 1979).
31. McRee, D. E. A visual protein crystallographic software system for X11/Xview. *J. Mol. Graphics* **10**, 44 (1992).
32. Cowtan, K. Joint CCP4 *ESF-EACBM Newsl. Protein Crystallogr.* **31**, 34 (1994).
33. Jones, T. A., Zou, J.-Y. Cowan, S. W. & Kjelgaard, M. Improved methods for the building of protein models in electron density maps and the location of errors in these. *Acta Crystallogr.* **A47**, 110–119 (1991).
34. Read, R. J. Improved Fourier coefficients for maps using phases from partial structures with errors. *Acta Crystallogr.* **42**, 140–149 (1986).
35. Brünger, A.T., *X-PLOR v3.8* (Yale University Press, New Haven, CT; 1996).
36. Kraulis, P. J. MOLSCRIPT- a program to produce both detailed and schematic plots of protein structures. *J. Appl. Crystallogr.* **24**, 946–950 (1991).
37. Nicholls, A., Sharp, K. A. & Honig, B. Protein folding and association: insights from the interfacial and thermodynamic properties of hydrocarbons. *Proteins: Struct. Funct. Genet.* **11**, 281–296 (1991).